DOI 10.1007/s10946-023-10151-9
Journal of Russian Laser Research, Volume 44, Number 4, July, 2023

EVOLUTION PROPERTIES OF A PARTIALLY COHERENT LAGUERRE PULSED VECTOR VORTEX BEAM IN A TURBULENT ATMOSPHERE WITH ANISOTROPY

Bangzhuo An, Yonggen Xu,* Wenli Liu, Nianchi Hao, Yongtao Liu, and Xueru Deng

Department of Physics, School of Science
Key Laboratory of High Performance Scientific Computation
Xihua University
Chengdu 610039, China

Corresponding author e-mail: xuyonggen06@126.com

Abstract

Based on the extended Huygens–Fresnel principle, we derive the analytical expression of the cross-spectral density matrix of a partially coherent Laguerre pulsed vector vortex beam (PCLPVVB) propagating through isotropic and anisotropic atmospheric turbulence. Our outcomes reveal that the atmospheric turbulence affects the evolution of spectral intensity distribution of PCLPVVB, and the beam quickly degenerates on propagation in the strong turbulence. We also can find that PCLPVVB with a larger topological charge has a stronger ability to resist the degeneration caused by atmospheric turbulence in comparison with the non-vortex beam. In addition, increasing the initial coherence length and mode order can increase the anti-turbulence ability of PCLPVVB, and the pulse duration significantly affects the spectral intensity of PCLPVVB in turbulence. Our research results are important for some applications in laser radar detection, remote sensing, and free-space optical communication.

Keywords: partially coherent Laguerre pulsed vector vortex beam, pulse duration, spectral intensity, anisotropic atmospheric turbulence.

1. Introduction

In recent years, the propagation characteristics of partially coherent (PC) beams, which have lower coherence, have received much attention [1–8]. Compared with fully coherent beams, partially coherent beams are widely used in theoretical research and practical applications, such as laser radar, spectral analysis, holographic technology, and other fields, because of their unique spectral intensity distribution and better propagation characteristics [9–14]. In 1992, Allen [15] proposed that, for a vortex beam with helical phase front, each photon can carry an orbital angular momentum (OAM) of $m\hbar$, where m is the topological charge carried by the beam and $\hbar$ is the reduced Planck constant. Using OAM coding or OAM multiplexing, the channel capacity of the optical communication system can be significantly improved, which makes vortex beam to have a strong application value in the free-space optical communication (FSOC) [16, 17]. As is commonly well known, Laguerre–Gaussian (LG) beams have been found to provide a greater capability in effectively reducing turbulence-induced scintillation [18–20]; they have a wide range of applications, such as LiDAR detection, holographic imaging, and biomedicine [21–23]. Besides, it is found that non-uniformly polarized beam, such as a radially polarized beam, exhibits a better ability to reduce the turbulence effects caused by atmospheric turbulence than linearly polarized

Manuscript submitted by the authors in English on February 24, 2023.

light [4, 24, 25]. On the other hand, a pulsed laser is widely used in high-speed optical communications, spectrographic detections, laser processing, medical surgery, and other fields because of its rich spectral content and high peak power [26–28]. In recent years, the propagation characteristics of pulsed beams in atmospheric turbulence have also received attention and research [7, 29, 30].

As we all know, atmospheric turbulence greatly influences the beam propagation, resulting in various turbulence effects, such as the light intensity scintillation, beam spreading, beam drift, and so on [18–20, 29, 30], which reduces the beam quality. Thus, improving the diminution of beam quality caused by atmospheric turbulence, when the beam is propagating, is very important. Generally, atmospheric turbulence is considered isotropic [1, 7, 8, 12]. However, some experiments show that atmospheric turbulence can be anisotropic. Anisotropic atmospheric turbulence was first proposed by Toselli [31] in 2014, in view of the use of anisotropic factors.

However, as far as we know, the propagation characteristics of partially coherent Laguerre pulsed vector vortex beam (PCLPVVB) in atmospheric turbulence have not been reported. In this paper, we study the evolution properties of PCLPVVB in anisotropic atmospheric turbulence. The effects of anisotropic factors, topological charges, initial coherent length, pulse duration, and mode order on the evolution of spectral intensity distribution for the PCLPVVB are discussed in detail. Our research results, presented in this paper, can provide a theoretical basis for reducing the impact of atmospheric turbulence on LiDAR detection.

2. Theoretical Formulation

The second-order evolution characteristics of PCLPVVB at points $\boldsymbol{\rho}_1' = (x_1', y_1')$ and $\boldsymbol{\rho}_2' = (x_2', y_2')$ and at different instant times t_1 and t_2 on the source plane ($z = 0$) can be generally characterized by a 2×2 two-point two-time mutual coherent function matrix (MCFM); it reads [20, 29]

$$\mathbf{\Gamma}^{(0)}(\boldsymbol{\rho}_1', \boldsymbol{\rho}_2', 0; t_1, t_2) = \begin{bmatrix} \Gamma_{xx}^{(0)}(\boldsymbol{\rho}_1', \boldsymbol{\rho}_2', 0; t_1, t_2) & \Gamma_{xy}^{(0)}(\boldsymbol{\rho}_1', \boldsymbol{\rho}_2', 0; t_1, t_2) \\ \Gamma_{yx}^{(0)}(\boldsymbol{\rho}_1', \boldsymbol{\rho}_2', 0; t_1, t_2) & \Gamma_{yy}^{(0)}(\boldsymbol{\rho}_1', \boldsymbol{\rho}_2', 0; t_1, t_2) \end{bmatrix}, \tag{1}$$

where $\Gamma_{\alpha\beta}^{(0)}(\boldsymbol{\rho}_1', \boldsymbol{\rho}_2', 0; t_1, t_2) = F_{\alpha\beta}(\boldsymbol{\rho}_1', \boldsymbol{\rho}_2', 0) \times G(t_1, t_2)(\alpha, \beta = x, y)$, $F_{\alpha\beta}(\boldsymbol{\rho}_1', \boldsymbol{\rho}_2', 0)$ represents a function related to spatial coordinates, and $G(t_1, t_2)$ represents a function related to time expressed as in [18, 20, 29, 32]; they read

$$\begin{aligned} F_{\alpha\beta}(\boldsymbol{\rho}_1', \boldsymbol{\rho}_2', 0) = {} & \frac{\alpha_1'\beta_2'}{2^{2m+4n}(n!w_0)^2} \exp\left[-\frac{\boldsymbol{\rho}_1'^2 + \boldsymbol{\rho}_2'^2}{w_0^2} - \frac{(\boldsymbol{\rho}'_1 - \boldsymbol{\rho}'_2)^2}{2\delta_{\alpha\beta}^2}\right] \\ & \times \sum_{a_1=0}^{n}\sum_{a_2=0}^{m}\sum_{a_3=0}^{n}\sum_{a_4=0}^{m} i^{a_4}(i^{a_2})^* \binom{n}{a_1}\binom{m}{a_2}\binom{n}{a_3}\binom{m}{a_4} \\ & \times H_{2a_1-a_2+m}\left(\frac{\sqrt{2}x_1'}{w_0}\right) H_{2a_2-a_4+m}\left(\frac{\sqrt{2}x_2'}{w_0}\right) H_{-2a_1+a_2+2n}\left(\frac{\sqrt{2}y_1'}{w_0}\right) H_{-2a_3+a_4+2n}\left(\frac{\sqrt{2}y_2'}{w_0}\right) \end{aligned} \tag{2}$$

and

$$G(t_1, t_2) = \exp[-i\omega_0(t_2 - t_1)] \exp\left[-\frac{t_1^2 + t_2^2}{2T_0^2} - \frac{(t_1 - t_2)^2}{2T_c^2}\right], \tag{3}$$

where n and m represent the mode order and the topological charge, respectively, w_0 denotes the waist width for the beam, $\delta_{\alpha\beta}$ is the spatial coherence length, $*$ is the complex conjugation, $H(\cdot)$ is the Hermite polynomial; also, $\begin{pmatrix} n \\ a_1 \end{pmatrix}$ and $\begin{pmatrix} m \\ a_2 \end{pmatrix}$ and $\begin{pmatrix} n \\ a_3 \end{pmatrix}$ and $\begin{pmatrix} m \\ a_4 \end{pmatrix}$ are the binomial coefficients, where ω_0 is the central angular frequency of the pulse, with T_0 being the pulse duration and T_c, the temporal coherence length.

Consider the Fourier transform [20, 29]

$$W_{\alpha\beta}(\boldsymbol{\rho'}_1, \boldsymbol{\rho'}_2, 0; \omega_1, \omega_2) = \iint F_{\alpha\beta}(\boldsymbol{\rho'}_1, \boldsymbol{\rho'}_2, 0) G(t_1, t_2) \times \exp\left[-i(\omega_2 t_2 - \omega_1 t_1)\right] dt_1\, dt_2, \tag{4}$$

where $W_{\alpha\beta}(\boldsymbol{\rho}'_1, \boldsymbol{\rho}'_2, 0; \omega_1, \omega_2)(\alpha, \beta = x, y)$ are the elements of the 2×2 two-point two-frequency cross-spectral density matrix (CSDM) in the source plane ($z = 0$). Then, the CSDM of PCLPVVB on the source plane can be written as follows [18, 29, 33]:

$$\begin{aligned} W_{\alpha\beta}(\boldsymbol{\rho'}_1, \boldsymbol{\rho'}_2, 0; \omega_1, \omega_2) = {} & \frac{T_0^3 T_c^2}{2\pi\sqrt{T_c^2 + 2T_0^2}} \exp\left\{-\frac{T_0^2 T_c^2 \left[(\omega_1 - \omega_0)^2 + (\omega_2 - \omega_0)^2\right]}{2T_c^2 + 4T_0^2}\right\} \\ & \times \exp\left[-\frac{T_0^4(\omega_1 - \omega_2)^2}{2T_c^2 + 2T_0^2}\right] \frac{\alpha'_1 \beta'_2}{2^{2m+4n}(n! w_0)^2} \exp\left[-\frac{\boldsymbol{\rho'}_1^2 + \boldsymbol{\rho'}_2^2}{w_0^2} - \frac{(\boldsymbol{\rho'}_1 - \boldsymbol{\rho'}_2)^2}{2\delta_{\alpha\beta}^2}\right] \\ & \times \sum_{a_1=0}^{n} \sum_{a_2=0}^{m} \sum_{a_3=0}^{n} \sum_{a_4=0}^{m} i^{a_4} (i^{a_2})^* \begin{pmatrix} n \\ a_1 \end{pmatrix} \begin{pmatrix} m \\ a_2 \end{pmatrix} \begin{pmatrix} n \\ a_3 \end{pmatrix} \begin{pmatrix} m \\ a_4 \end{pmatrix} \\ & \times H_{2a_1 - a_2 + m}\left(\frac{\sqrt{2}x'_1}{w_0}\right) H_{2a_2 - a_4 + m}\left(\frac{\sqrt{2}x'_2}{w_0}\right) H_{-2a_1 + a_2 + 2n}\left(\frac{\sqrt{2}y'_1}{w_0}\right) H_{-2a_3 + a_4 + 2n}\left(\frac{\sqrt{2}y'_2}{w_0}\right). \end{aligned} \tag{5}$$

Let $\omega_1 = \omega_2 = \omega$, then according to the generalized Huygens–Fresnel principle, when a PCLPVVB propagates in atmospheric turbulence, the two-point CSDM in the received plane can be characterized as [7, 29, 33, 34]:

$$W_{\alpha\beta}(\boldsymbol{\rho}, \boldsymbol{\rho}_d, z; \omega) = \left(\frac{1}{\lambda z}\right)^2 \iiiint W_{\alpha\beta}(\boldsymbol{\rho'}, \boldsymbol{\rho}'_d, 0; \omega) \exp\left\{\frac{ik}{z}\left[(\boldsymbol{\rho} - \boldsymbol{\rho'})(\boldsymbol{\rho}_d - \boldsymbol{\rho}'_d)\right]\right\} \cdot \langle \exp(\psi_1 + \psi_2^*)\rangle d^2\boldsymbol{\rho'}\, d^2\boldsymbol{\rho}'_d, \tag{6}$$

where $\boldsymbol{\rho} = (\boldsymbol{\rho}_1 + \boldsymbol{\rho}_2)/2$, $\boldsymbol{\rho'} = (\boldsymbol{\rho}'_1 + \boldsymbol{\rho}'_2)/2$, $\boldsymbol{\rho}_d = \boldsymbol{\rho}_1 - \boldsymbol{\rho}_2$, $\boldsymbol{\rho}'_d = \boldsymbol{\rho}'_1 - \boldsymbol{\rho}'_2$, $\boldsymbol{\rho} = (x, y)$, $\boldsymbol{\rho}_d = (x_d, y_d)$, $\boldsymbol{\rho'} = (x', y')$, and $\boldsymbol{\rho}'_d = (x'_d, y'_d)$, with $\boldsymbol{\rho}_1 = (x_1, y_1)$ and $\boldsymbol{\rho}_2 = (x_2, y_2)$ being the positions of two points in the received plane, respectively. Also, here, λ represents the wavelength of the beam, $k = 2\pi/\lambda$ is the wave number, z represents the propagation distance, $\langle\cdot\rangle$ represents the ensemble average, and $\langle \exp(\psi_1 + \psi_2^*)\rangle$ is the turbulent factor, which can be approximately written as [18, 30, 33]

$$\langle \exp(\psi_1 + \psi_2^*)\rangle \approx \exp\left[-\frac{\boldsymbol{\rho}_d^2 + \boldsymbol{\rho}_d \cdot \boldsymbol{\rho}'_d + \boldsymbol{\rho'}_d^2}{\rho_0^2}\right]. \tag{7}$$

Here, ρ_0 is the coherence length of a spherical wave propagating in atmospheric turbulence, which reads [18, 30, 33]

$$\rho_0 = \left[\frac{1}{3}\pi^2 k^2 z \int_0^\infty \varkappa^3 \Phi_n(\varkappa)\, d\varkappa\right]^{-1/2}, \tag{8}$$

and $\Phi_n(\varkappa)$ represents the spatial power spectrum of the refractive-index fluctuations of anisotropic atmospheric turbulence, which is [18, 24, 29, 35, 36]

$$\Phi_n(\varkappa) = \frac{A(\alpha)\tilde{C}_n^2\xi_x\xi_y}{(\xi_x^2\varkappa_x^2 + \xi_y^2\varkappa_y^2 + \varkappa_z^2 + \varkappa_0^2)^{\alpha/2}} \exp\left(-\frac{\xi_x^2\varkappa_x^2 + \xi_y^2\varkappa_y^2 + \varkappa_z^2}{\varkappa_m^2}\right), \qquad (3 < \alpha < 4), \tag{9}$$

where ξ_x and ξ_y denote the anisotropic factors. Also, $A(\alpha) = [\Gamma(\alpha-1)\cos(\alpha\pi/2)]/(4\pi^2)$, where $\Gamma(\cdot)$ is the gamma function and α is the generalized exponent parameter, $\tilde{C}_n^2$ is the generalized refractive-index structure parameter with units $\mathrm{m}^{3-\alpha}$, $\varkappa_x$, $\varkappa_y$, and $\varkappa_z$ are three components of the spatial wave number $\varkappa$ along the x, y, and z directions, $\varkappa_0 = 2\pi/L_0$ and $\varkappa_m = c(\alpha)/l_0$, with L_0 and l_0 being the outer scale and inner scale of turbulence, respectively, and $c(\alpha) = [2\pi A(\alpha)\Gamma(5/2-\alpha/2)/3]^{1/(\alpha-5)}$.

Substituting Eqs. (5) and (7)–(9) into Eq. (6) provides the possibility to express the CSDM of a PCLPVVB propagating through the anisotropic atmospheric turbulence as follows:

$$\begin{aligned} W_{xx}(\boldsymbol{\rho}, \boldsymbol{\rho}_d, z; \omega) = {} & \frac{T_0^3 T_c^2 \pi}{2\sqrt{T_c^2 + 2T_0^2}} \exp\left[-\frac{T_0^2 T_c^2 (\omega-\omega_0)^2}{T_c^2 + 2T_0^2}\right] \frac{1}{2^{2m+4n}(n!w_0)^2} \left(\frac{1}{\lambda z}\right)^2 \\ & \times \exp\left(-\frac{ik\boldsymbol{\rho}\cdot\boldsymbol{\rho}_d}{z}\right) \exp\left(-\frac{\boldsymbol{\rho}_d^2}{\rho_0^2}\right) \sum_{a_1=0}^{n}\sum_{a_2=0}^{m}\sum_{a_3=0}^{n}\sum_{a_4=0}^{m} \\ & \times \sum_{b_1=0}^{[a_1-a_2/2+m/2]} \sum_{b_2=0}^{1+2a_1-a_2-2b_1+m} \sum_{b_3=0}^{[b_2/2]} \sum_{b_4=0}^{[a_3-a_4/2+m/2]} \sum_{c_1=0}^{-2a_1+a_2+2n} \sum_{c_2=0}^{[c_1/2]} \sum_{c_3=0}^{[n-a_3+a_4/2]} (i^{a_2})^* \\ & \times i^{a_4-2m-2n+a_2-2a_1+4b_1+2b_3+4b_4-c_1+4c_2+4c_3-2} \Omega_1\Omega_2 N_{1xx} N_{2xx} E_{xx} \\ & \times H_{\Delta_1}\left(\sqrt{\frac{2}{A_{1xx}}} iK_{xx}\right) H_{\Delta_2}\left(\frac{\sqrt{2}}{A_{4xx}} K_{yy}\right) H_{\Delta_3}\left(\frac{iQ_{xx}}{2\sqrt{A_{3xx}}}\right) H_{\Delta_4}\left(\frac{iR_{xx}}{2\sqrt{A_{3xx}}}\right) \end{aligned} \tag{10}$$

and

$$\begin{aligned} W_{yy}(\boldsymbol{\rho}, \boldsymbol{\rho}_d, z; \omega) = {} & \frac{T_0^3 T_c^2 \pi}{2\sqrt{T_c^2 + 2T_0^2}} \exp\left[-\frac{T_0^2 T_c^2 (\omega-\omega_0)^2}{T_c^2 + 2T_0^2}\right] \frac{1}{2^{2m+4n}(n!w_0)^2} \left(\frac{1}{\lambda z}\right)^2 \exp\left(-\frac{ik\boldsymbol{\rho}\cdot\boldsymbol{\rho}_d}{z}\right) \\ & \times \exp\left(-\frac{\boldsymbol{\rho}_d^2}{\rho_0^2}\right) \sum_{a_1=0}^{n}\sum_{a_2=0}^{m}\sum_{a_3=0}^{n}\sum_{a_4=0}^{m} \\ & \times \sum_{b_1=0}^{2a_1-a_2+m} \sum_{b_2=0}^{[b_1/2]} \sum_{b_3=0}^{[a_3-a_4/2+m/2]} \sum_{b_4=0}^{[n-a_1+a_2/2]} \sum_{c_1=0}^{-2a_1+a_2-2b_4+2n+1} \sum_{c_2=0}^{[c_1/2]} \sum_{c_3=0}^{[n-a_3+a_4/2]} (i^{a_2})^* \\ & \times i^{a_4-m-4n-a_2+2a_1-b_1+4b_2+4b_3+4b_4+2c_2+4c_3-2} \Omega_3\Omega_4 N_{1yy} N_{2yy} E_{yy} \\ & \times H_{\Delta_5}\left(\sqrt{\frac{2}{A_{1yy}}} iK_{yy}\right) H_{\Delta_6}\left(\frac{\sqrt{2}}{A_{4yy}} K_{xx}\right) H_{\Delta_7}\left(\frac{iQ_{yy}}{2\sqrt{A_{3yy}}}\right) H_{\Delta_8}\left(\frac{iR_{yy}}{2\sqrt{A_{3yy}}}\right), \end{aligned} \tag{11}$$

where

$$A_{1xx}=\frac{1}{w_0^2}+\frac{1}{2\delta_{xx}^2}+\frac{1}{\rho_0^2}+\frac{ik}{2z},\quad A_{2xx}=\frac{1}{2\delta_{xx}^2}+\frac{1}{\rho_0^2},\quad A_{3xx}=A_{1xx}^*-\frac{A_{2xx}^2}{A_{1xx}},\quad A_{4xx}=\sqrt{\frac{1}{2}w_0^2A_{1xx}^2-A_{1xx}},$$

$$K_{xx}=-\frac{x_d}{2\rho_0^2}+\frac{ik}{2z}\left(x+\frac{x_d}{2}\right),\quad K_{yy}=-\frac{y_d}{2\rho_0^2}+\frac{ik}{2z}\left(y+\frac{y_d}{2}\right),\quad L_{xx}=\frac{x_d}{2\rho_0^2}-\frac{ik}{2z}\left(x+\frac{x_d}{2}\right),$$

$$L_{yy}=\frac{y_d}{2\rho_0^2}-\frac{ik}{2z}\left(y+\frac{y_d}{2}\right),\quad Q_{xx}=L_{xx}+\frac{A_{2xx}K_{xx}}{A_{1xx}},\quad R_{xx}=L_{yy}+\frac{A_{2xx}K_{yy}}{A_{1xx}},$$

$$A_{1yy}=\frac{1}{w_0^2}+\frac{1}{2\delta_{yy}^2}+\frac{1}{\rho_0^2}+\frac{ik}{2z},\quad A_{2yy}=\frac{1}{2\delta_{yy}^2}+\frac{1}{\rho_0^2},\quad A_{3yy}=A_{1yy}^*-\frac{A_{2yy}^2}{A_{1yy}},\quad A_{4yy}=\sqrt{\frac{1}{2}w_0^2A_{1yy}^2-A_{1yy}},$$

$$Q_{yy}=L_{xx}+\frac{A_{2yy}K_{xx}}{A_{1yy}},\quad R_{yy}=L_{yy}+\frac{A_{2yy}K_{yy}}{A_{1yy}},$$

$$\Omega_1=\begin{pmatrix} n \\ a_1 \end{pmatrix}\begin{pmatrix} m \\ a_2 \end{pmatrix}\begin{pmatrix} n \\ a_3 \end{pmatrix}\begin{pmatrix} m \\ a_4 \end{pmatrix}\begin{pmatrix} 1+2a_1-a_2-2b_1+m \\ b_2 \end{pmatrix}\begin{pmatrix} -2a_1+a_2+2n \\ c_1 \end{pmatrix},$$

$$\Omega_2=\frac{b_2!c_1!(2a_1-a_2+m)!(2a_3-a_4+m)!(-2a_3+a_4+2n)!}{b_1!b_3!b_4!c_2!c_3!(b_2-2b_3)!(c_1-2c_2)!(2a_1-a_2+m-2b_1)!(2a_3-a_4+m-2b_4)!(-2a_3+a_4+2n-2c_3)!}$$

$$N_{1xx}=\left(\sqrt{2}\right)^{2b_1-m-2n-5}\left(\sqrt{A_{1xx}}\right)^{2a_1-a_2+2b_1-b_2+2b_3-m-4n-3}\left(\sqrt{2}A_{2xx}\right)^{b_2-2b_3+c_1-2c_2},$$

$$N_{2xx}=\left(\frac{w_0}{\sqrt{2}}\right)^{2b_1+2b_4+2c_3-2m-4n}\left(\sqrt{A_{3xx}}\right)^{-b_2+2b_3+2b_4-c_1+2c_2+2c_3-m-2n-3}\left(A_{4xx}\right)^{a_2-2a_1+c_1+2c_2+2n},$$

$$\Omega_3=\begin{pmatrix} n \\ a_1 \end{pmatrix}\begin{pmatrix} m \\ a_2 \end{pmatrix}\begin{pmatrix} n \\ a_3 \end{pmatrix}\begin{pmatrix} m \\ a_4 \end{pmatrix}\begin{pmatrix} 2a_1-a_2+m \\ b_1 \end{pmatrix}\begin{pmatrix} -2a_1+a_2-2b_4+2n+1 \\ c_1 \end{pmatrix},$$

$$\Omega_4=\frac{b_1!c_1!(2a_3-a_4+m)!(2n-2a_1+a_2)!(-2a_3+a_4+2n)!}{b_2!b_3!b_4!c_2!c_3!(b_1-2b_2)!(c_1-2c_2)!(2a_3-a_4+m-2b_3)!(2n-2a_1+a_2-2b_4)!(2n-2a_3+a_4-2c_3)!}$$

$$N_{1yy}=\left(\sqrt{2}\right)^{2b_4-m-2n-5}\left(\sqrt{A_{1yy}}\right)^{2a_1-a_2-2b_4+c_1-2c_2+2m+2n+3}\left(\sqrt{2}A_{2yy}\right)^{b_1-2b_2+c_1-2c_2},$$

$$N_{2yy}=\left(\frac{w_0}{\sqrt{2}}\right)^{2b_3+2b_4+2c_3-2m-4n}\left(\sqrt{A_{3yy}}\right)^{-b_1+2b_2+2b_3-c_1+2c_2+2c_3-m-2n-3}\left(A_{4yy}\right)^{-a_2+2a_1-b_1+2b_2+m},$$

$$E_{xx}=\exp\left(\frac{K_{xx}^2+K_{yy}^2}{A_{1xx}}\right)\exp\left(\frac{Q_{xx}^2+R_{xx}^2}{4A_{3xx}}\right),\quad E_{yy}=\exp\left(\frac{K_{xx}^2+K_{yy}^2}{A_{1yy}}\right)\exp\left(\frac{Q_{yy}^2+R_{yy}^2}{4A_{3yy}}\right),$$

$$\Delta_1=2a_1-a_2-2b_1-b_2+m+1,\quad \Delta_2=-2a_1+a_2-c_1+2n,$$

$$\Delta_3=2a_3-a_4+b_2-2b_3-2b_4+m+1,\quad \Delta_4=-2a_3+a_4+c_1-2c_2-2c_3+2n,$$

$$\Delta_5=2n-2a_1+a_2-2b_4+1-c_1,\quad \Delta_6=2a_1+m-a_2-b_1,$$

$$\Delta_7=2a_3+m-a_4+b_1-2b_2-2b_3,\quad \Delta_8=2n-2a_3+a_4+c_1-2c_2-2c_3+1. \tag{12}$$

In order to study the spectral density, we assume $\boldsymbol{\rho}_d=0$ in Eqs. (10)–(12); on the observation plane, it is given by [7, 18, 24]

$$S(\boldsymbol{\rho},z;\omega)=W_{xx}(\boldsymbol{\rho},z;\omega)+W_{yy}(\boldsymbol{\rho},z;\omega). \tag{13}$$

In view of Eqs. (10)–(13), we can study the spectral intensity of the PCLPVVB propagating through atmospheric turbulence.

3. Numerical Simulation and Discussion

In this section, we use the above analysis to numerically calculate the spectral intensity of PCLPVVB in isotropic and anisotropic atmospheric turbulence. We set the calculation parameters as follows: $w_0 = 0.015$ m, $\lambda = 632.8$ nm, $\omega_0 = 2.9788$ rad/fs, $\omega = 1.01\omega_0$, $l_0 = 8$ mm, $L_0 = 80$ m, and $\alpha = 11/3$. The remaining parameters are listed in the captures to figures.

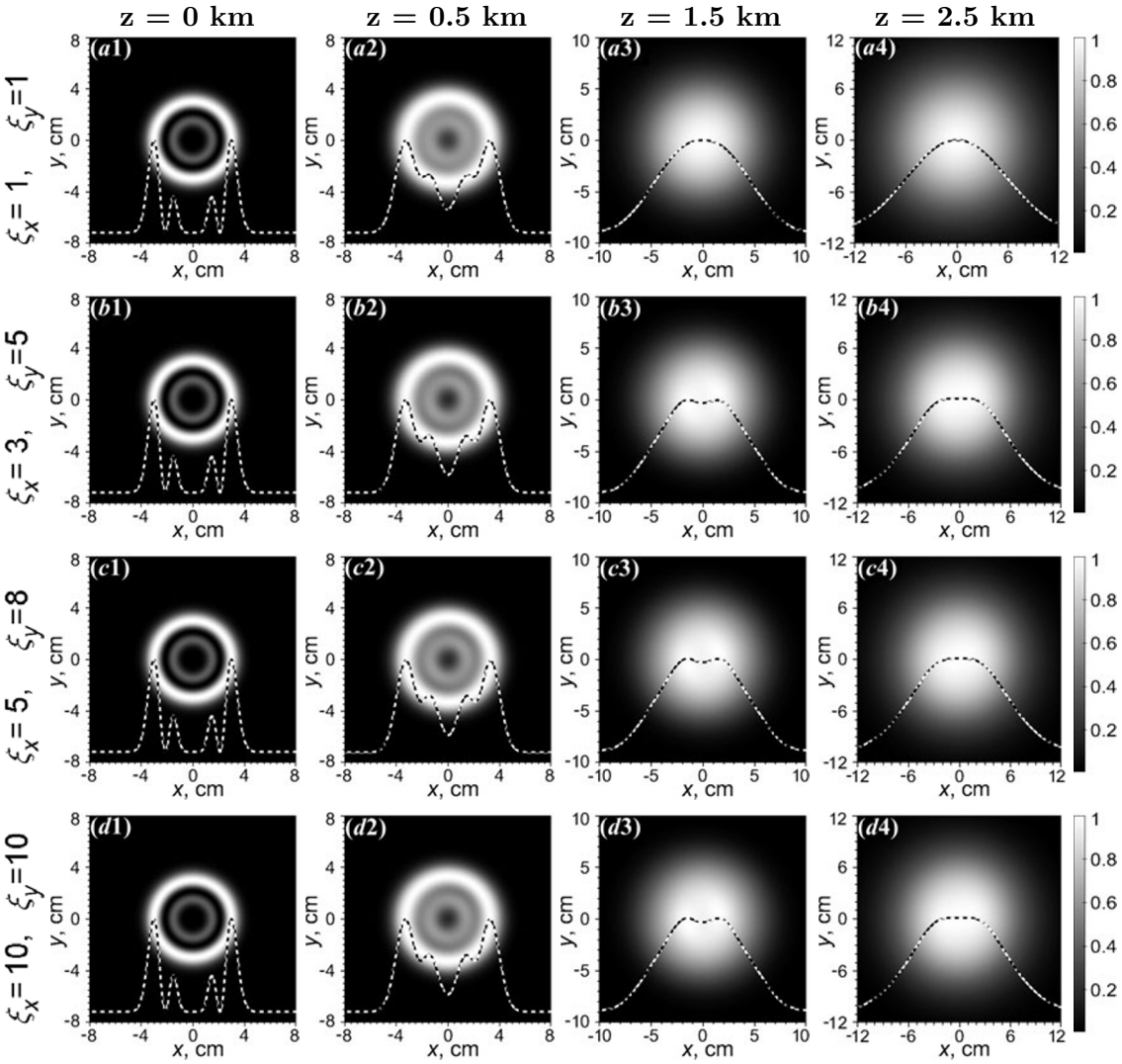

Fig. 1. Normalized spectral intensity distributions of the PCLPVVB at several propagation distances z in isotropic atmospheric turbulence and anisotropic atmospheric turbulence for different anisotropic factors ξ_x and ξ_y. Here. $\delta_{xx} = 0.01$ m, $\delta_{yy} = 0.012$ m, $\tilde{C}_n^2 = 1 \cdot 10^{-14}$ m$^{3-\alpha}$, $n = 1$, $m = 3$, $T_0 = 80$ fs, and $T_c = 50$ fs.

In Fig. 1, we display the normalized spectral intensity distributions of PCLPVVB with different anisotropic factors ξ_x and ξ_y in isotropic and anisotropic atmospheric turbulence at different propagation distances z. In Fig. 1 a1, b1, c1, d1, we can see that the spectral intensity of the PCLPVVB is distributed in the source plane in multi-ring dark hollow, and the intensity of the outer ring is greater than that of the inner ring. Also, in Fig. 1 a1, a2, a3, a4, we can see that, as the propagation distance increases, the

beam spreads gradually, and the hollow region gradually disappears in isotropic atmospheric turbulence. Then, the normalized spectral intensity distribution for the beam evolves into a flat-topped distribution and eventually degenerates into a Gaussian-like distribution. In Fig. 1 H1–H4, where H = b, c, d, we find that the evolution properties of PCLPVVB in anisotropic atmospheric turbulence are similar to those in isotropic atmospheric turbulence. However, because of increase in ξ_x and ξ_y, i.e., the decrease of atmospheric turbulence intensity, the degradation of the beam from multi-ring dark hollow distribution to Gaussian-like distribution is decelerated. This is due to the fact that, when the atmospheric turbulence is weakened, its destruction to the spatial coherence of the beam is reduced.

In Fig. 2, we show the normalized spectral intensity distributions of PCLPVVB at different propagation distances z in isotropic atmospheric turbulence under different topological charges m. One can see in Fig. 2 a1, a2, a3, a4, that when the topological charge $m = 0$, the beam degenerates from PCLPVVB

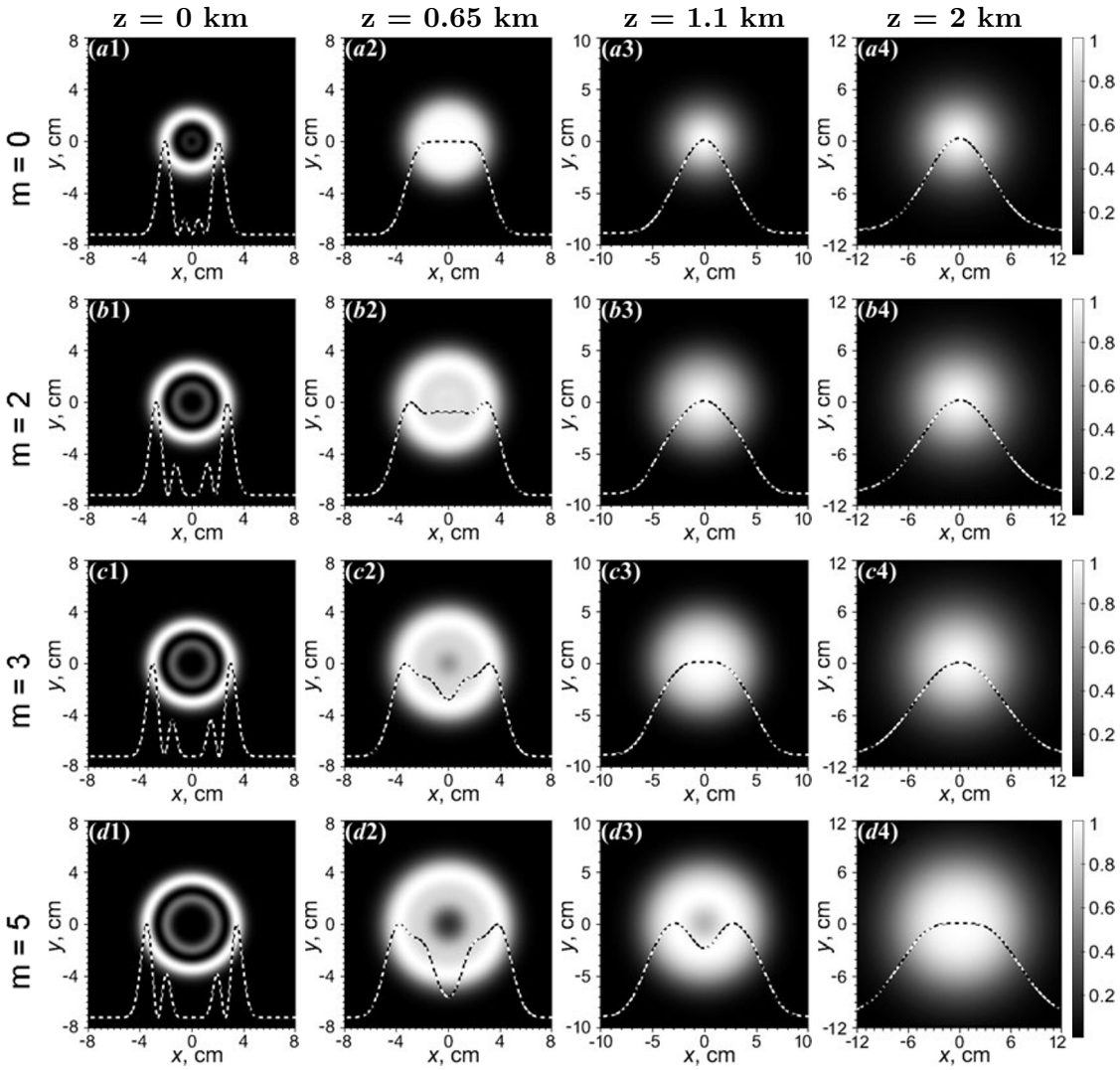

Fig. 2. Normalized spectral intensity distributions of PCLPVVB at different propagation distances z in isotropic atmospheric turbulence with different topological charges m. Here, $\delta_{xx} = \delta_{yy} = 0.01$ m, $\tilde{C}_n^2 = 1 \cdot 10^{-14}$ m$^{3-\alpha}$, $\xi_x = \xi_y = 1$, $n = 1$, $T_0 = 80$ fs, and $T_c = 50$ fs.

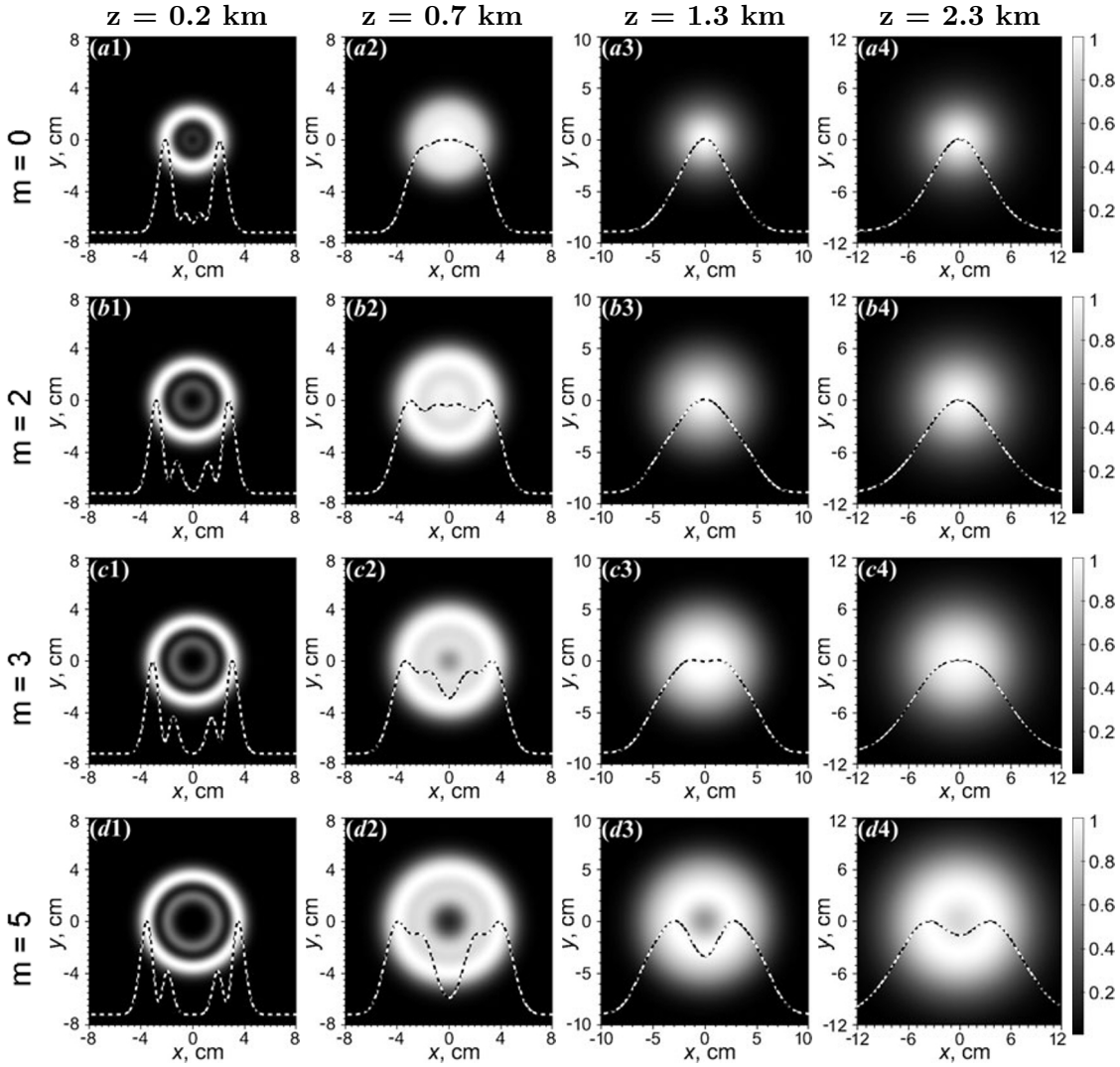

Fig. 3. Normalized spectral intensity distributions of PCLPVVB at different propagation distances z in anisotropic atmospheric turbulence with different topological charges m. Here, $\delta_{xx} = \delta_{yy} = 0.01$ m, $\tilde{C}_n^2 = 1 \cdot 10^{-14}$ m$^{3-\alpha}$, $\xi_x = \xi_y = 10$, $n = 1$, $T_0 = 80$ fs, and $T_c = 50$ fs.

to a partially coherent Laguerre pulsed vector non-vortex beam. With increase in the propagation distance z, the beam spreads gradually and, at $z = 0.65$ km, the beam changes from a hollow beam to a flat-topped beam. As the beam continues to propagate in turbulent atmosphere, the normalized spectral intensity distribution of the beam eventually degenerates into a Gaussian-like distribution. Comparing all normalized spectral intensity distributions shown in Fig. 2 a1, b1, c1, and d1, we can find that, when the topological charge m increases, the outer ring, inner ring, and hollow region of the light spot on the source plane also increase. In addition, we find that the topological charge m greatly influences the evolution speed of the beam in atmospheric turbulence. For the PCLPVVB, the process of its degradation in turbulent atmosphere is decelerated, especially when m is large. For example, when $m = 3$, the normalized spectral intensity distribution of the beam is flat-topped distribution at $z = 1.1$ km and becomes Gaussian-like distribution at $z = 2$ km. But at $m = 5$, the beam turns into a flat-topped beam at $z = 2$ km. Importantly, it displays that PCLPVVB with a larger topological charge has a stronger

ability to resist the degeneration caused by atmospheric turbulence in comparison with the non-vortex beam.

In Fig. 3, we display normalized spectral intensity distributions of PCLPVVB at different propagation distances z in anisotropic atmospheric turbulence, where we increase the anisotropy factor, ξ_x and ξ_y, to 10, which is the weaker atmospheric turbulence. Comparing Figs. 3 and 2, we can state that, in weaker atmospheric turbulence, the evolution of the beam will be slower, and the propagation distance z, at which the normalized spectral intensity distribution degenerates into flat-topped distribution and Gaussian-like distribution, will be longer. We also find that, in weak turbulence, the rate at which the beam evolves into a Gaussian-like shape slows down more with increase in the topological charge m.

In Fig. 4, we show the normalized spectral intensity distributions of PCLPVVB at different propagation distances z under different initial coherence lengths δ_{xx} and δ_{yy} in anisotropic atmospheric turbulence. In Fig. 4 b2, c2, we can see that, when δ_{xx} and δ_{yy} are not equal, the inner ring of the light

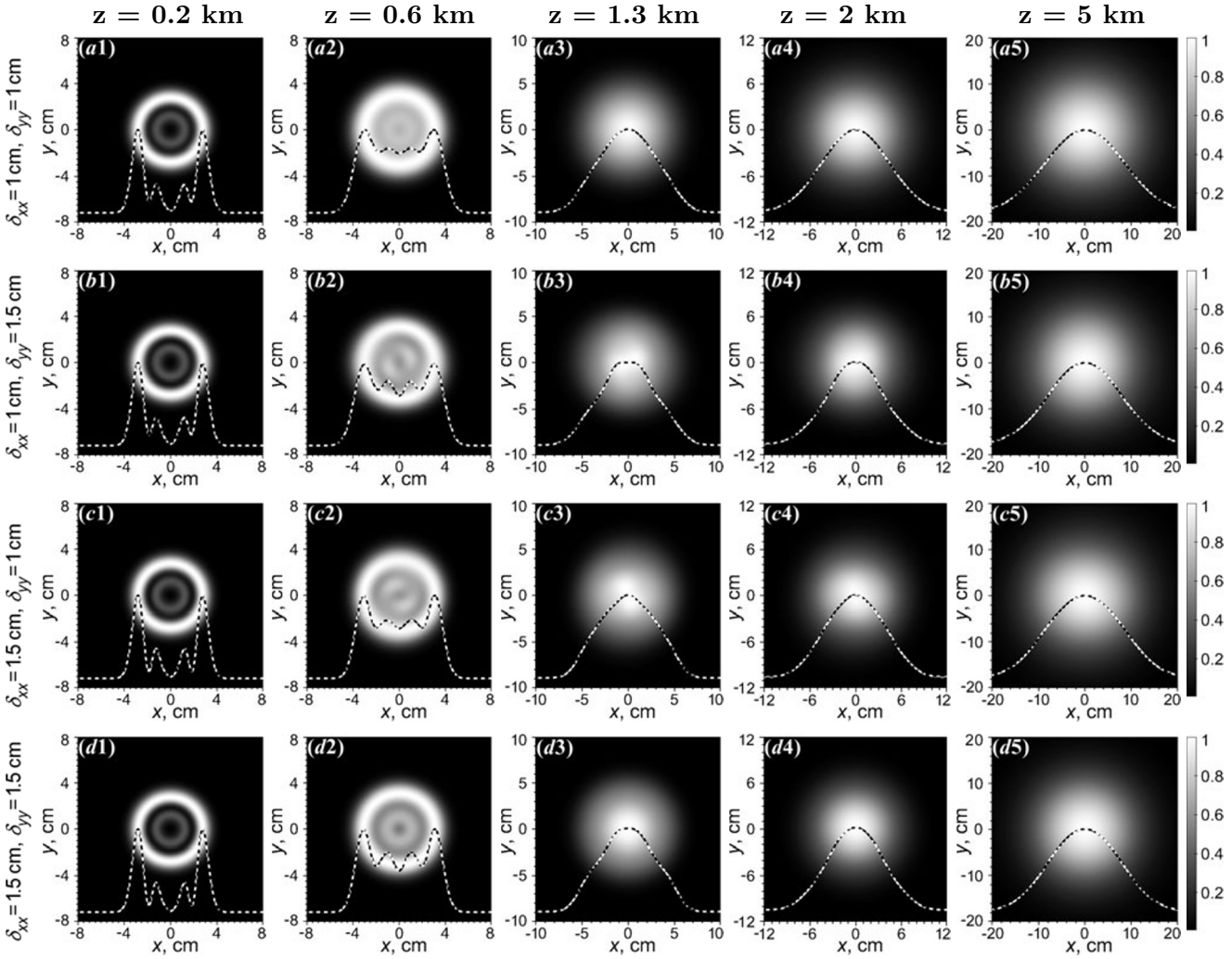

Fig. 4. Normalized spectral intensity distribution of PCLPVVB at different propagation distances z in anisotropic atmospheric turbulence under different initial coherence lengths δ_{xx} and δ_{yy}. Here, $\tilde{C}_n^2 = 1 \cdot 10^{-14}$ m$^{3-\alpha}$, $\xi_x = 3$, $\xi_y = 5$, $n = 1$, $m = 2$, $T_0 = 80$ fs, and $T_c = 50$ fs.

spot splintered. This is because atmospheric turbulence damages the transverse coherence of the beam to a different extent, causing the beam to expand along the x and y directions in different degrees. At the same time, from Fig. 4 K1–K4, where K = a, b, c, d, one can see that, when the coherence length increases, the evolution of the beam is slowing down. Therefore, an appropriate increase in the initial coherence length of the beam can increase the anti-turbulence ability of PCLPVVB. When the beam propagates to a longer distance, as shown in Fig. 4 K5, even if the initial coherence lengths are not equal, the distribution of PCLPVVB gradually changes from elliptical distribution to circular distribution. This is due to the fact that atmospheric turbulence regulates the coherence of the beam, so that the expansion of the beam along the x and y directions gradually tends to be the same, when the beam propagates to a longer distance.

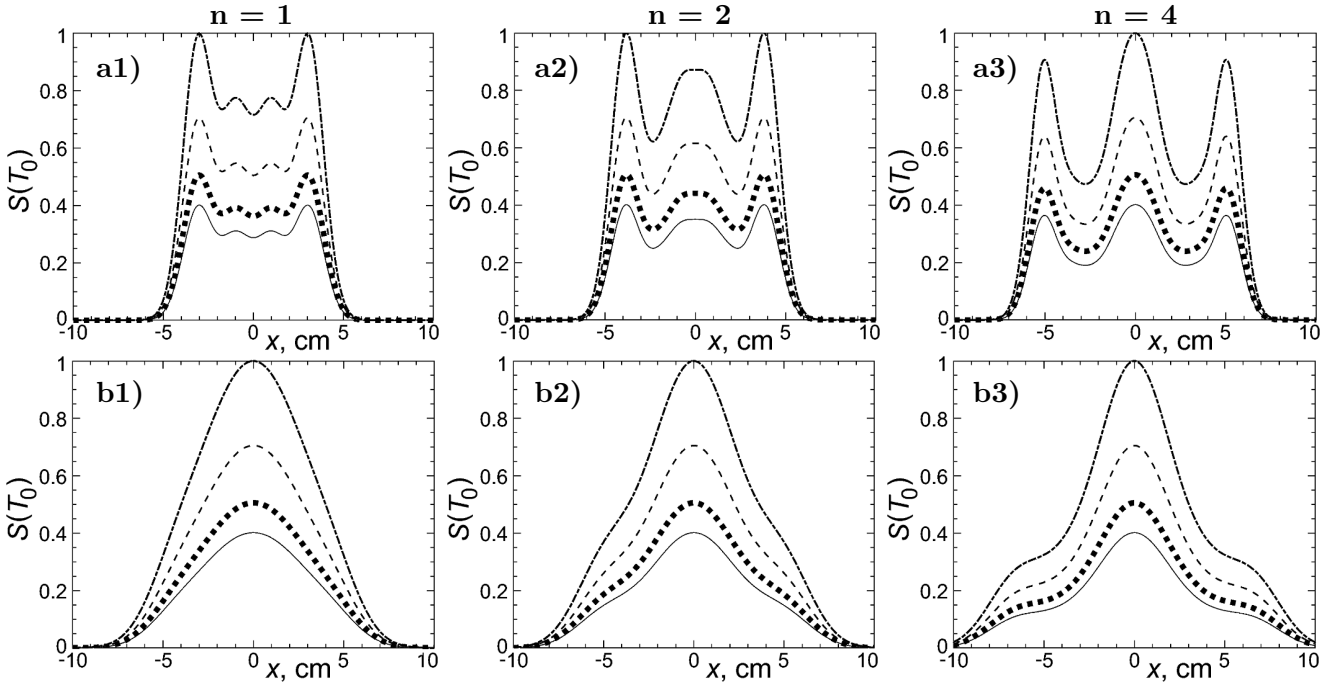

Fig. 5. The relationship between the normalized spectral intensity with the pulse duration of the PCLPVVB propagating through the anisotropic turbulence for different mode orders n. Here, $\delta_{xx} = \delta_{yy} = 0.01$ m, $\tilde{C}_n^2 = 1 \cdot 10^{-14}$ m$^{3-\alpha}$, $m = 2$, and $\xi_x = \xi_y = 10$, $T_0 = 40$ fs (solid curves), $T_0 = 50$ fs (dotted curves), $T_0 = 70$ fs (dashed curves), and $T_0 = 100$ fs (dash-dotted curves), $z = 0.6$ km (a) and $z = 1.3$ km (b).

In Fig. 5, we show the $S(T_0)$ of PCLPVVB propagating through the anisotropic turbulent atmosphere at different propagation distances z under different pulse durations. The normalized spectral intensity $S(T_0) = S(\boldsymbol{\rho}, z; \omega)/S_{\max}(\boldsymbol{\rho}, z; \omega)$ was used for comparison purposes, where $S_{\max}(\boldsymbol{\rho}, z; \omega)$ is the maximum spectral intensity of points $\boldsymbol{\rho}$ at a pulse duration of 100 fs. One can see that the pulse duration significantly affects the spectral intensity of PCLPVVB; the overall $S(T_0)$ increases with increase in the pulse duration T_0. In Fig. 5 L1, L2, L3, where L = a, b, we find that, at the same distance, the beam spot increases as the mode order n increases. When $z = 0.6$ km, since the intensity of the inner ring of the beam is greater when the mode order n is larger, the beam can no longer maintain a dark hollow after n increases. At the same time, we also find that, as the propagation distance increases, the evolution speed of the beam is slower when n is larger. This indicates that at a larger mode order n the beam is less affected by atmospheric turbulence.

4. Summary

In this paper, we studied in detail the evolution properties of a partially coherent Laguerre pulsed vector vortex beam propagating through isotropic and anisotropic atmospheric turbulence. We discussed the effects of anisotropy factor, topological charge, initial coherence length, pulse duration, and mode order on the evolution of spectral intensity distribution of PCLPVVB propagating through turbulent atmosphere. We found that the spectral intensity of PCLPVVB on the source plane was multi-ring dark hollow distribution, and with increase in the propagation distance, the normalized spectral intensity distribution for the beam evolves into a flat-topped distribution and eventually degenerated into a Gaussian-like distribution. When ξ_x and ξ_y increased, i.e., the intensity of atmospheric turbulence decreased, the degradation of the beam from multi-ring dark hollow distribution to Gaussian-like distribution decelerated. When the topological charge m was larger, the evolution speed of the beam was slower, i.e., PCLPVVB with a larger topological charge had a stronger ability to resist the degeneration caused by atmospheric turbulence in comparison with the non-vortex beam. Also, we found that in weak turbulence, the rate at which the beam evolved into a Gaussian-like shape slowed down more with increase in the topological charge m. When the initial coherence length δ_{xx} and δ_{yy} were not equal, the inner ring of the light spot appeared splitting phenomenon due to the different degrees of expansion of the beam along the x and y directions, and the evolution speed of the beam slowed down when the coherence length increased. Therefore, an appropriate increase in the initial coherence length of the beam can increase the anti-turbulence ability of PCLPVVB. The value of the spectral intensity of PCLPVVB increases with increase in the pulse duration T_0. At the same time, as the propagation distance increases, the evolution speed of the beam is slower when mode order n is larger, which indicates that PCLPVVB has a stronger anti-turbulence ability at a larger mode order n. Thus, PCLPVVB may have potential applications for reducing the impact of atmospheric turbulence on LIDAR detection and free-space optical communication.

Acknowledgments

This work is supported by the Department of Science and Technology of Sichuan Province under Grants Nos. 2021YJ0518 and 2019YJ0470, the Sichuan Provincial University Key Laboratory of Detection and Application of Space Effect in Southwest Sichuan under Grant No. ZDXM202201003, the National Natural Science Foundation of China (NSFC) under Grant No. 11703011, and the Yunnan Key Laboratory of Solar Physics and Space Science under Grant No. YNSPCC202202.

References

1. J. L. Zhao, G. Q. Wang, Y. Yin, et al., *Optik*, **241**, 167237 (2021).
2. Y. Xu, Y. G. Xu, S. J. Wang, et al., *J. Russ. Laser Res.*, **43**, 509 (2022).
3. S. Rasouli, E. M. Razi, and J. J. Niemela, *J. Opt. Soc. Am. A*, **39**, 1641 (2022).
4. K. Huang, Y. G. Xu, J. Cao, et al., *J. Russ. Laser Res.*, **44**, 110 (2023).
5. Q. Li, *J. Mod. Opt.*, **68**, 1221 (2021).
6. X. Guo, C. Yang, M. L. Duan, et al., *Optik*, **243**, 167361 (2021).
7. Y. G. Xu, Y. Q. Dan, J. Y. Yu, et al., *J. Mod. Opt.*, **64**, 1976 (2017).
8. Q. Xu, L. Zhao, and Y. G. Xu, *Optik*, **265**, 169542 (2022).
9. Y. Baykal, Y. Ata, and M. C. Gokce, *Appl. Opt.*, **60**, 2166 (2021).

10. Q. C. Yang, T. S. Wang, J. D. Chen, et al., *Opt. Commun.*, **496**, 127078 (2021).
11. L. Zhu, A. D. Wang, M. L. Deng, et al., *Opt. Express*, **29**, 32580 (2021).
12. J. L. Zhao, G. Q. Wang, X. L. Ma, et al., *Photonics*, **8**, 5 (2021).
13. Y. Wu, H. P. Mei, C. M. Dai, et al., *Opt. Commun.*, **472**, 126041 (2020).
14. X. X. Zhou, Z. Y. Zhou, P. Tian, et al., *Appl. Opt.*, **58**, 9443 (2019).
15. L. Allen, M. W. Beijersbergen, R. J. C. Spreeuw, et al., *Phys. Rev. A.*, **45**, 8185 (1992).
16. G. Gibson, J. Courtial, M. J. Padgett, et al., *Opt. Express*, **12**, 5448 (2004).
17. J. Wang, J. Y. Yang, I. M. Fazal, et al., *Nat. Photonics*, **6**, 488 (2012).
18. Y. Xu, L. Zhao, N. Yang, et al., *J. Mod. Opt.*, **69**, 200 (2022).
19. M. T. Xie, J. Y. Wang, J. H. Li, et al., *J. Mod. Opt.*, **69**, 728 (2022).
20. Y. Xu, Y. G. Xu, and T. J. Wang, *Photonics*, **9**, 707 (2022).
21. G. A. Swartzlander, *Opt. Lett.*, **26**, 497 (2001).
22. B. Melo, I. Brandao, B. P. da Silva, et al., *Phys. Rev. Appl.*, **14**, 034069 (2020).
23. M. Y. Luo, D. Q. Sun, Y. J. Yang, et al., *Opt. Commun.*, **463**, 125434 (2020).
24. L. Zhao, Y. G. Xu, and S. K. Yang, *Optik*, **227**, 166115 (2021).
25. M. J. Cheng, L. X. Guo, and J. T. Li, *J. Quant. Spectrosc. Radiat. Transf.*, **218**, 12 (2018).
26. X. F. Cai, P. Gu, and Z. X. Zhang, *J. Russ. Laser Res.*, **43**, 169 (2022).
27. J. Wei, P. X. Jin, X. C. Cao, et al., *Chin. Opt. Lett.*, **20**, 041405 (2022).
28. Y. K. Wang, K. W. Geng, T. Chen, et al., *J. Russ. Laser Res.*, **43**, 201 (2022).
29. Y. Li, M. Gao, and B. Li, *Opt. Commun.*, **518**, 128385 (2022).
30. K. L. Yong, J. W. Yan, S. M. Huang, et al., *Optik*, **180**, 27 (2019).
31. I. Toselli, *J. Opt. Soc. Am. A.*, **31**, 1868 (2014).
32. Y. G. Xu, Y. D. Li, and X. L. Zhao, *J. Opt. Soc. Am. A.*, **32**, 1623 (2015).
33. L. Zhao, Y. G. Xu, and Y. Q. Dan, *Opt. Express*, **29**, 34986 (2021).
34. Y. Q. Dan and B. Zhang, *Opt. Express*, **16**, 15563 (2008).
35. J. Wang, S. J. Zhu, H. Y. Wang, et al., *Opt. Express*, **24**, 11626 (2016).
36. M. J. Cheng, L. X. Guo, J. T. Li, et al., *J. Opt. Soc. Am. A.*, **33**, 1442 (2016).